## RESEARCH ARTICLE

# A Denoising Method for Loaded Coal-Rock Charge Signals Based on a Joint Algorithm of IWT and ICEEMDAN

**XIN LI[1], JINGRAN BU[1], ZHEN YANG[1], HAO LI[1], HUI ZUO[2], YUNING WANG[3], AND JING ZHOU[1]**

[1]Faculty of Electrical and Control Engineering, Liaoning Technical University, Huludao 125105, China
[2]Taxation Bureau of Gongchangling District, State Administration of Taxation, Liaoyang 111008, China
[3]Dalian Vocational Technical College, Dalian 116035, China

Corresponding author: Jingran Bu (15041880263@163.com)

**ABSTRACT** The electromagnetic radiation signal generated by loaded coal and rock is widely used to predict coal and rock dynamic disasters. However, due to the presence of significant electromagnetic interference at the coal mine site, the accuracy of the collected signals is insufficient. For the collected noisy charge induction signals, the wavelet threshold function of traditional denoising methods has problems such as non-progressiveness and discontinuity at the threshold. In order to achieve a better signal noise reduction effect, this paper proposes a collection based on an improved wavelet threshold (IWT) function and an improved complete ensemble empirical mode decomposition with adaptive noise (ICEEMDAN) combined denoising algorithm. It overcomes mode aliasing and optimizes signal smoothness. Firstly, the algorithm is used to decompose the noisy signal and calculate the intrinsic mode function (IMF) and correlation coefficient of each order to distinguish the noise from the correlated signal. Then, the IMF component dominated by the signal is reconstructed to complete the denoising. The simulation and experimental results show that this algorithm can effectively remove noise in charge induction signals, and its signal-to-noise ratio (SNR) is improved by 2.3482 and 0.095 compared to six algorithms such as IWT and VMD, respectively. Compared with four algorithms, including the improved threshold function and the improved threshold function combined with Ensemble Empirical Mode Decomposition (EEMD), its noise-to-noise ratio (Rnn) decreased by 3.112, showing good noise reduction performance. The results presented in this paper provide a new method for collecting real charge induction signals.

**INDEX TERMS** Charge induction signal, improved complete ensemble empirical mode decomposition with adaptive noise, improved wavelet threshold, combined denoising.

## I. INTRODUCTION

As a major source of energy, coal mining safety issues have become increasingly prominent in its mining process. In order to reduce the occurrence of such disasters, coal and rock dynamic disaster prediction has received a lot of attention. There is a clear signature of charge-induced signals in the fracture process of the coal-rock. However, the charge-induced signals collected in coal mining are characterized by randomness, abruptness, and wide frequency bands. As a result, the collected charge-induced signal is often mixed with various noise disturbances, which affects

The associate editor coordinating the review of this manuscript and approving it for publication was Dominik Strzalka.

the realism of signal extraction [1]. In this complex form, conventional denoising techniques have struggled to meet the requirements. In order to accurately study the variation law of the charge-induced signal during coal fracture and to better obtain the predictive properties of the signal, it is necessary to explore denoising algorithms with higher SNR. Therefore, the study of new denoising methods has become an inevitable trend.

At present, the most commonly used signal decomposition method with wavelet decomposition [2] and empirical mode decomposition (EMD) [3]. Among them, wavelet transform methods can provide the time-frequency localization properties of signals. But the choice of wavelet basis functions and thresholds is problematic. Due to the wide and complex sources of signal noise. This can easily lead to certain limitations in its adaptability when processing complex engineering signals [4], [5]. Compared with wavelet transform method, EMD method does not need to select wavelet basis function or decomposition layer, but it has some problems such as false mode components and mode aliasing, so it has some limitations in practical application. EEMD improves the pattern confusion problem of EMD algorithms by repeatedly adding different white noise to the original signal [6], [7], however, the added white noise can lead to reconstruction errors. CEEMD can introduce reverse white noise into the target signal, thus effectively reducing the reconstruction error of EEMD. However, if the white noise added is not appropriate in amplitude and number of iterations, the result will be not accurate [8], [9]. Therefore, domestic and foreign scholars have carried out a lot of research on signal denoising methods on this basis, and achieved certain theoretical results: Xie et al. [10] investigated a modified wavelet threshold calculation method and threshold treatment function. This prevents the usual bias caused by traditional soft thresholding methods and reduces the bias due to inaccurate thresholds. Moreover, it solves the discontinuity of the traditional hard threshold function. Li et al. [11] employed different decomposition layers, analyzed the denoising effect of different decomposition layers, compared the SNR and the mean values, and finally obtained the optimal denoising layer as 4 layers, which can achieve good denoising effect. Gu et al. [12] proposed a hybrid algorithm based on wavelet packet transformation-BP neural network, which used wavelet packet transform to filter the energy feature extraction and decomposition and reconstruction capabilities of the signal, and then carried out preliminary decomposition and reconstruction of the transient electromagnetic signal to obtain the final transient electromagnetic signal. Bayer et al. [13] introduced an adaptive filtering procedure called SpcShrink that can significantly distinguish the wavelet coefficients of the signal of interest. Deng and Zhang [14] proposed an improved threshold function, which was compared with hard threshold, soft threshold and existing threshold functions, and concluded that the function had superior mathematical characteristics.

The superiority of the algorithm was verified by the objective evaluation method of peak SNR and MSE. Zhang et al. [15] adopted a method to remove image noise, mainly using the improved threshold function to apply the wavelet coefficient to the high-frequency part of threshold processing, and then obtain the de-noised image to reconstruct the image. Kumar et al. [16] studied the denoising technology using stationary wavelet transform, which retained more ECG signal components and was superior to other ECG denoising methods. Zhong et al. [17] proposed a method to select threshold parameters or the number of decomposition layers without human intervention in order to achieve the denoising effect of electrical signals. Hou and Guo [18] proposed a denoising method based on modified complementary integrated empirical mode decomposition (MCEEMD), which has good adaptability and can suppress the mode aliasing of EMD to a certain extent. Jia et al. [19] proposed a new method of vibration signal denoising based on EEMD and grey theory, called EEMD-Gray, which can effectively remove noise and retain useful information. Jin et al. [20] adopted a novel adaptive integrated empirical mode decomposition (NAEEMD) denoising method based on partial discharge, which has good denoising effect and effectiveness. Cheng et al. [21] adopted the EEMD method to distinguish the intrinsic mode function (IMF) of noise and signal, and removed the IMF whose main component was noise, and then used the SVD-LWT method to remove the noise in the IMF component containing signal, so as to extract signal in a fine manner. Dao et al. [22] proposed an adaptive modulation interval threshold denoising algorithm based on empirical mode decomposition, and finally raised the SNR by 1-3dB. Compared with direct empirical mode decomposition denoising method and traditional threshold denoising method, the root-mean-square error was reduced by 10-25%. Zhang et al. [23] proposed a new denoising method based on convolutional neural network with long short-term memory (CNN-LSTM) and CEEMD, which improved the accuracy of signal measurement. Li et al. [24] adopted an adaptive denoising method based on the combination of wavelet threshold based on EEMD and singular spectrum analysis (SSA). This method can significantly reduce the MSE, and the overall denoising effect is better than EEMD and wavelet threshold denoising algorithms. Xiong et al. [25] proposed a denoising method based on variational mode decomposition (VMD) and wavelet threshold for speech signals with noise. Sun et al. [26] improved the wavelet threshold method and combined it with EEMD algorithm for denoising to ensure the availability of signals. Feng et al. [27] adopted ICEEMDAN and improved wavelet Threshold (IWT) hierarchical decomposition to improve the signal separation effect and achieve signal noise reduction. The above studies have improved the wavelet thresholding algorithm and the EMD algorithm. These can overcome the drawbacks of poor selectivity and universality of wavelet bases, as well as mode aliasing in EMD. However, due to the complex environment of the mine

site, the electromagnetic signals are greatly affected during the collection process, resulting in their reduced quality. Continued improvement of the noise reduction performance of the signal is still necessary in order to make the precursor signal of electromagnetic radiation more accurate in predicting dynamical disasters in coal rocks.

The electromagnetic radiation method, as one of the existing geophysical monitoring methods, is helpful for predicting coal rock dynamic disasters [28]. Due to the complex coal mine environment, electromagnetic signals are severely disturbed during signal acquisition. This increases the difficulty of extracting the signal features and drastically reduces its predictive performance. Currently, scholars have achieved some results in the study of noise reduction of electromagnetic radiation signals: Huang et al. [29] uses the iterative thresholding approach of the wavelet transform for denoising. The noise is removed from the signal by thresholding. Based on this, an analysis of the generation law of electromagnetic radiation during the failure of sandstone impacts was performed. Yang et al. [30] proposed a new electromagnetic radiation signal denoising algorithm that combines Adaptive Ensemble Empirical Mode Decomposition (AEEMD) and Improved Wavelet Transform (IWT). This algorithm optimizes both soft and hard threshold formulations, overcomes the wavelet basis selection and decomposition layer problems, and has certain advantages. Safta et al. [31] used wavelet functions to denoise the electromagnetic radiation signals generated by microcontrollers under harsh conditions and obtained good physical data. Wu et al. [32] proposed a noise denoising algorithm based on variational Bayesian-based adaptive Kalman filter (VBAKF) for electromagnetic data subjected to mixed noise interference. It effectively suppresses noise in the data. Chen and Wang [33] proposed a method of EEMD adaptive morphological filters to eliminate electromagnetic signals collected by coal rock dynamic disaster systems, in order to improve the accuracy of electromagnetic signals. The above algorithm sets the stage for studying the denoising of electromagnetic radiation signals. However, there is still relatively little research on related content at this stage. In particular, the research on denoising methods for predicting the signal of dynamical disasters in coal and rocks is not yet mature. This is not conducive to the development of coal and rock dynamic disaster prevention and control.

In view of the above shortcomings, in order to better remove the noise in charge induction signals, this paper proposes an improved wavelet threshold combined with ICEEMDAN algorithm, and then uses simulation signals and experimental signals to verify its denoising effect. At the same time, SNR and RMSE are used to compare the denoising effect of this algorithm with other algorithms, and further verify the superiority of this algorithm. The research results can be used for better processing of noisy signals and provide technical support for the research of coal and rock dynamic disaster prevention methods.

## II. IWT AND ICEEMDAD ALGORITHM
### A. IMPROVED THRESHOLD DENOISING ALGORITHM
The principle of wavelet threshold denoising is to determine a limit value and distinguish the noise from the original signal by comparing the size with the wavelet coefficient: when the wavelet coefficient is numerically high, it is considered effective, and the hard threshold method gives it the original value retention processing, and the soft threshold gives it the contraction to 0 according to certain rules. On the contrary, it is considered to represent noise and should be disposed of [34] and [35]. In order not to change the overall trend of the signal, the wavelet coefficients generally keep the low-frequency part of the signal and only process the high-frequency part of each layer.

After the hard threshold is processed, the wavelet coefficient is denoted as

$$\hat{\omega}_{c,k} = \begin{cases} \omega_{c,k} & |\omega_{c,k}| \geq \lambda \\ 0 & else \end{cases} \tag{1}$$

After soft threshold processing, the wavelet coefficient is denoted as

$$\hat{\omega}_{c,k} = \begin{cases} sign\left(\omega_{c,k}\right)\left(|\omega_{c,k}| - \lambda\right) & |\omega_{c,k}| \geq \lambda \\ 0 & else \end{cases} \tag{2}$$

where $\omega_{c,k}$ is the wavelet coefficient corresponding to the high frequency band after each layer wavelet decomposition; $\hat{\omega}_{c,k}$ is the estimated wavelet coefficient of the real signal; sign( ) is a symbolic function; $\lambda$ is a threshold.

Although the hard threshold denoising can effectively retain the original data of the wavelet coefficients, so as to completely restore the local details of the signal, the smoothness of the reconstructed signal is poor, which increases the difficulty of calculation. The soft threshold algorithm has continuity and ensures the smoothness of image edges, but it compresses the amplitude of effective wavelet coefficients, resulting in the loss of some high-frequency signals. To solve these problems, a new threshold function between hard and soft thresholds is constructed. The expression of the new threshold function is

$$\hat{\omega}_{c,k} = \begin{cases} sign\left(\omega_{c,k}\right)\left(|\omega_{c,k}|^{n} - \lambda^{n}\right)^{\frac{1}{n}} & \omega_{c,k} \geq \lambda \\ 0 & \omega_{c,k} < \lambda \end{cases} \tag{3}$$

where n $\geq$ 1.

The threshold function (3) is continuous like the soft threshold function and is higher-order derivable when $|\omega_{c,k}| > \lambda$. Examining the function

$$g(t) = sign(t)\left(|t|^{N} - \lambda^{N}\right)^{\frac{1}{N}} \tag{4}$$

where $N$ is the total number of wavelet coefficients.

Calculate the oblique asymptote of the function, and when t>0, the calculation result is

$$t > 0 \begin{cases} k = \lim_{t \to +\infty} \dfrac{g(t)}{t} = \lim_{t \to +\infty} \dfrac{\left(|t|^N - \lambda^N\right)^{\frac{1}{N}}}{t} \\ \qquad = \lim_{t \to +\infty} \left(1 - (\dfrac{\lambda}{t})^N\right)^{\frac{1}{N}} = 1 \\ b = \lim_{t \to +\infty} (g(t) - t) \\ \qquad = \lim_{t \to +\infty} \left(\left(|t|^N - \lambda^N\right)^{\frac{1}{N}} - t\right) = 0 \end{cases}$$
(5)

Similarly, when t<0 is calculated, it is

$$t < 0 \begin{cases} k = \lim_{t \to -\infty} \dfrac{g(t)}{t} = 1 \\ b = \lim_{t \to -\infty} (g(t) - t) = 0 \end{cases}$$
(6)

From functions (5) and (6), it can be concluded that function (4) takes the line y = t as its asymptote, so the threshold function (3) is asymptote to $\hat{\omega}_{c,k} = \omega_{c,k}$. With the increase of $\omega_{c,k}$, $\hat{\omega}_{c,k}$ can converge to $\omega_{c,k}$ indefinitely, which solves the problem of constant deviation of $\omega_{c,k}$ and $\hat{\omega}_{c,k}$ in the soft threshold denoising method, and improves the reconstruction accuracy.

Also, when $N \to +\infty$, if $\left|\omega_{c,k}\right| > \lambda$ then

$$\lim_{N \to +\infty} \hat{\omega}_{c,k} = sign\left(\omega_{c,k}\right)$$

$$\times \left|\omega_{c,k}\right| \lim_{N \to +\infty} \left(1 - \left(\dfrac{\lambda}{\left|\omega_{c,k}\right|}\right)^N\right)^{\frac{1}{N}}$$
$$= sign\left(\omega_{c,k}\right) \times \left|\omega_{c,k}\right| = \omega_{c,k}$$
(7)

Therefore, when N→ +∞, the IWT function is equivalent to the hard threshold function, and when N= 1, the IWT function is equivalent to the soft threshold function. It can be seen that the improved threshold function is a function that can adjust changes between the hard threshold function and the soft threshold function. When $\left|\omega_{c,k}\right| = \lambda$, $\hat{\omega}_{c,k} = 0$, and when $\left|\omega_{c,k}\right| \to \lambda$, then, $\left|\omega_{c,k}\right| \to 0$, that is, $\hat{\omega}_{c,k}$ is continuous at $\left|\omega_{c,k}\right| = \lambda$ and the deviation between $\hat{\omega}_{c,k}$ and $\left|\omega_{c,k}\right|$ decreases gradually as $\left|\omega_{c,k}\right|$ gradually increases. Therefore, the IWT function has better denoising effect compared to hard and soft thresholds, achieving higher signal reconstruction accuracy.

The specific steps to the IWT function denoising are as follows:
1) Wavelet basis selection: Performing orthogonal wavelet transform on noisy signals to determine a suitable set of wavelet decomposition coefficients $\hat{\omega}_{c,k}$.
2) Determine threshold λ: On the basis of calculating the standard deviation of noise, the threshold is obtained by solving.

$$\lambda = \delta\sqrt{2\ln N}$$
(8)
$$\delta = \dfrac{\alpha_D}{y}$$
(9)

where $\delta$ is the noise standard deviation; $\alpha_D$ is the noise standard deviation.
(3) Threshold processing: with λ Perform threshold processing on $\omega_{c,k}$ for the threshold, and obtain the estimated value $\hat{\omega}_{c,k}$ of the wavelet coefficients through formula (3).
(4) Wavelet reconstruction: Using an improved threshold function to reconstruct the unprocessed low-frequency band and the wavelet coefficients of $\hat{\omega}_{c,k}$, obtaining the final reconstructed signal.

Through the analysis, the graph of the IWT function is obtained and compared with the soft threshold and hard threshold function, as shown in Figure 1, it can be found that the hard threshold function is interrupted between $-\lambda$ and $\lambda$ which leads to poorer smoothing and increased computation after signal reconstruction. The soft threshold function improves the intermittent shortcomings of the hard threshold function, reducing the computational effort and ensuring smoothness of the reconstructed signal. However, the disadvantage is that the coefficient amplitude of the effective signal is compressed, resulting in the loss of high-frequency signal, with a fixed difference between $\omega_{c,k}$ and $\hat{\omega}_{c,k}$, and its contraction to 0 according to the rule will make the details of the signal not be restored, and the signal distortion occurs [36], [37], [38], [39]. In contrast, the IWT function smoothes the curves without interruption and preserves the signal intact. But its selection of threshold is important, and the denoising effect will be limited by it.
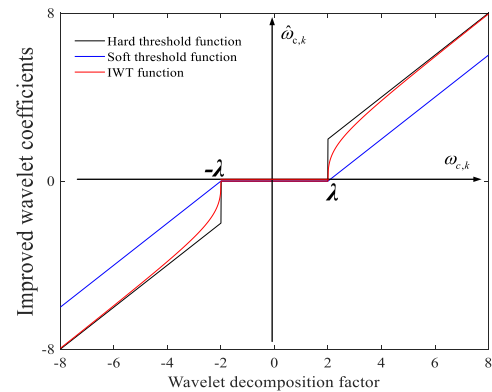


FIGURE 1. IWT function graph.

B. IMPROVED ADAPTIVE NOISE SET EMPIRICAL MODE DECOMPOSITION

EMD algorithm decomposes non-stationary nonlinear signals into intrinsic mode functions (IMF) with smooth characteristics from high to low, but IMF may have mode confusion caused by abnormal events. EEMD algorithm is an improvement of EMD algorithm, by adding several orders of white noise to the original signal, and EMD for the combined message, but it is found that the decomposition result is incomplete. The complete ensemble empirical mode decomposition with adaptive noise (CEEMDAN) algorithm can not only reduce the number of screening, In addition, ICEEMDAN also avoids the problem that the difference of

IMF decomposition results among groups in CEEMD makes it difficult to align the final set average, but at the same time, there are shortcomings, and ICEEMDAN solves the problem of residual noise and pseudo-modes in CEEMDAN.

ICEEMDAN employs adaptive noise and full integration strategy to improve the stability and accuracy of the decomposition. In this algorithm, the initial signal is decomposed into multiple IMFs, and each IMF is denoised using an adaptive denoising algorithm. The final denoised IMFs are integrated to obtain the resolved signal.

The ICEEMDAN algorithm can decompose the signal into several more accurate IMF components, which selects the $k$th IMF component of the Gaussian white noise decomposed by EMD in the decomposition process, denoted by $E_k(\cdot)$; while the first $IMF_1$ is related to the residuals by the equation [40]:

$$IMF_1 = x - R_1 \tag{10}$$

where, x is the original signal; $R_1$ is a first-order residual, whose expression is:

$$R_1 = \left\langle N(x^{(i)}) \right\rangle \tag{11}$$

where $N(\cdot)$ denotes the operator for solving the local mean of the signal; $\langle\cdot\rangle$ is the operator for averaging throughout the computation; and $x^{(i)}$ is the signal after the addition of white noise, which is expressed as:

$$x^{(i)} = x + \beta_0 E_1(\omega^{(i)}[n]) \tag{12}$$

where $\omega^{(i)}[n]$ refers to the ith Gaussian white noise added (i=1,2,3,…i); $\beta_k$ is the SNR of the $k$ stage.

Continue to add white noise, using the local mean decomposition to calculate the residual of the second stage as:

$$R_2 = \left\langle N\left(R_1 + \beta_1 E_2\left(\omega^{(i)}\right)\right)\right\rangle \tag{13}$$

and define the second modal component of the signal $IMF_2$ as:

$$IMF_2 = R_1 - R_2 = R_1 - \left\langle N\left(R_1 + \beta_1 E_2\left(\omega^{(i)}[n]\right)\right)\right\rangle \tag{14}$$

calculate the kth residual as:

$$R_k = \left\langle N\left(R_{k-1} + \beta_{k-1} E_k\left(\omega^{(i)}[n]\right)\right)\right\rangle \tag{15}$$

and calculate the kth mode component as:

$$IMF_k = R_{k-1} - R_k \tag{16}$$

according to the above process, all modes and residuals are obtained until the end of decomposition. The specific decomposition procedure of the algorithm is shown in Fig. 2:
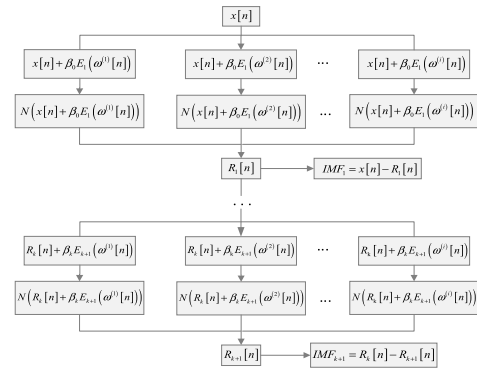


**FIGURE 2.** Flowchart of ICEEMD algorithm.

## III. STUDY OF JOINT EMR SIGNAL PROCESSING BY IWT AND ICEEMDAN
### A. JOINT IWT AND ICEEMDAN DENOISING ALGORITHM
The ICEEMDAN algorithm can effectively improve the mode aliasing phenomenon in the EMD algorithm, and adaptive signal processing has also been implemented [40]. The IWT denoising algorithm optimizes both the traditional soft and hard thresholds, allowing threshold denoising to achieve signal adaptation as well. The combination of the two can overcome the pickiness of wavelet bases and solve the problem of choosing and decomposing wavelet bases. Compared to the existing algorithms, the joint algorithm of IWT and ICEEMDAN for coal and rock signals has a significant advantage in protecting the peaks and abrupt signals of charge induction signals. It is suitable for denoising transient signals generated by coal rock fractures, and it can effectively distinguish high-frequency effective signals from high-frequency noise without missing high-frequency signals. Therefore, the joint algorithm of IWT and ICEEMDAN for charge induction signal denoising achieves significantly better performance.

The specific computational steps of the joint denoising algorithm of the IWT function and ICEEMDAN are as follows:

1) Perform ICEEMDAN decomposition of the noise-containing signal to obtain the IMF components of each order.

2) Calculate the correlation coefficient R of each order IMF component and noise-containing signal, establish the correlation coefficient curve, and set the order corresponding to the first local minima in the graph as k-order, and the components before k-order are mainly noise-dominated signals, and the components after k-order are mainly effective signals.

$$R(y(t), IMF_j) = \frac{cov(y(t), IMF_j)}{\sigma_{y(t)} \times \sigma_{IMF_j}} \tag{17}$$

where $cov(y(t), IMF_j)$ is the covariance between the noise-containing signal and each modal function; $\sigma_{y(t)}$ and $\sigma_{IMF_j}$ are their standard deviations.

3) The IMF components of each order are sequentially processed with improved threshold function to obtain the IMF components of each order after denoising.
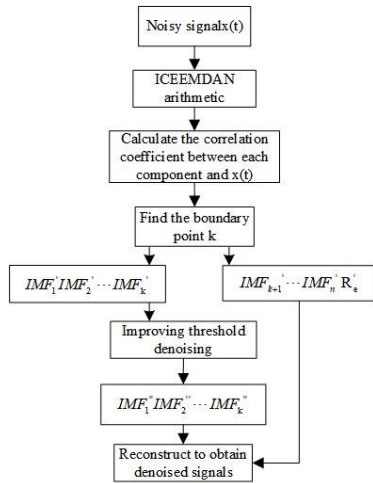
**FIGURE 4.** Original signal diagram.



**FIGURE 5.** Noise signal map.



**FIGURE 3.** Flow chart of joint denoising algorithm.

4) Signal reconstruction is performed on the effective signal components after the $k$th order to obtain the denoised signal.

The flowchart of the joint denoising algorithm is shown in Figure 3, and the reconstructed signal is:

$$\bar{f}_k(t) = \sum_{j=1}^{k} IMF_j''(t) + \sum_{j=k+1}^{n} IMF_j'(t) + R_e'(t) \quad (18)$$

where $IMF_j''(t)$ is the signal function of the noise dominated signal after denoising by the joint algorithm; $IMF_j'(t)$ is the effective signal function; $R_e'(t)$ is the residual.

## B. DE-NOISING SIMULATION VERIFICATION OF ADDITIVE NOISE SIGNAL.

When verifying the feasibility and superiority of the IWT function and ICEEMDAN joint denoising algorithm, for the convenience of observation, the waveform is continuous and periodic sinusoidal function signal is used for simulation, and its signal expression is:

$$x(t) = 2.5 \sin(2\pi f_1 t) + 3 \sin(2\pi f_2 t) \quad (19)$$

where $f_1$ is 0.7, $f_2$ is 0.05, the total number of sampling points is 3000, the wavelet basis function is sym6, and the number of solving layers is 3 layers. Due to the complexity of the noise generated by the environmental interference during the acquisition process, in order to verify the applicability of the algorithm in this paper, the noise-containing signal y($t$) obtained after adding random white noise $n(t)$ to the original signal is

$$y(t) = x(t) + n(t) \quad (20)$$

The simulation diagrams of the original signal and the noise added signal are shown below:

As can be seen from Fig.6, ICEEMDAN algorithm decomposes the noisy signal into 9 IMF components and a trend term (res). The results for each component are clear and there is no mode aliasing. Among them, IMF1 to IMF4 components
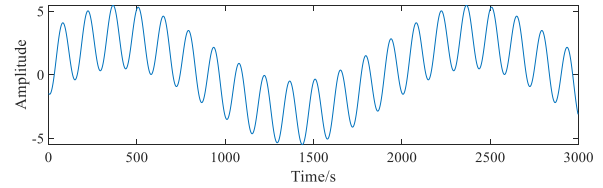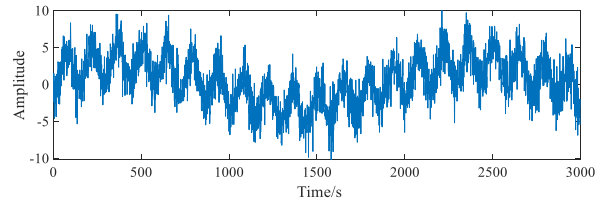
contain obvious noise, IMF5-IMF9 components contain less noise, which is closer to the real signal. The improved threshold function processing was carried out for each component, and the correlation coefficient between the processed IMF component and the noisy signal was calculated, and the correlation coefficient variation chart as shown in Fig. 7 was obtained. From Fig. 7, it can be seen that the image exhibits a fluctuating trend. The correlation coefficient of IMF5 is 0.5628, which serves as a boundary point to extract the fifth and subsequent IMF components for reconstruction. Finally, a smooth curve with periodic fluctuations is obtained, that is, the signal after noise removal.

In order to further demonstrate the accuracy and superiority of the denoising performance of IWT function and ICEEMDAN combined algorithm, IWT function, VMD algorithm, IWT and EMD combined algorithm, IWT and EEMD combined algorithm, and IWT and ICEEMDAN combined algorithm are respectively used to denoise the same simulation signal, and their denoising effects are compared. Figure 8 shows the comparison of the de-noising effects of the six algorithms. From the comparison of Figures 8 (a) - (f), it can be seen that the denoising effect of each algorithm gradually strengthens. The effect of denoising using the IWT and VMD algorithms is not ideal. There are still multiple burrs and oscillations in the signal. Comparing Fig 8 (a) and Fig 8 (c), it can be seen that the joint algorithm has a better denoising effect. After denoising using the joint algorithm of IWT and ICEEMDAN, it is evident that most of the signal spikes are filtered out. The smoothness of the signal is improved, making it closer to the original signal. And two evaluation criteria, SNR and mean square error (RMSE), are used to evaluate the denoising performance of the signal [41]. The calculation formula is as follows:

$$SNR = 10 \times \lg \left[ \frac{\sum_{i=1}^{n} (y_i)^2}{\sum_{i=1}^{n} (y_i - x_i)^2} \right] \quad (21)$$
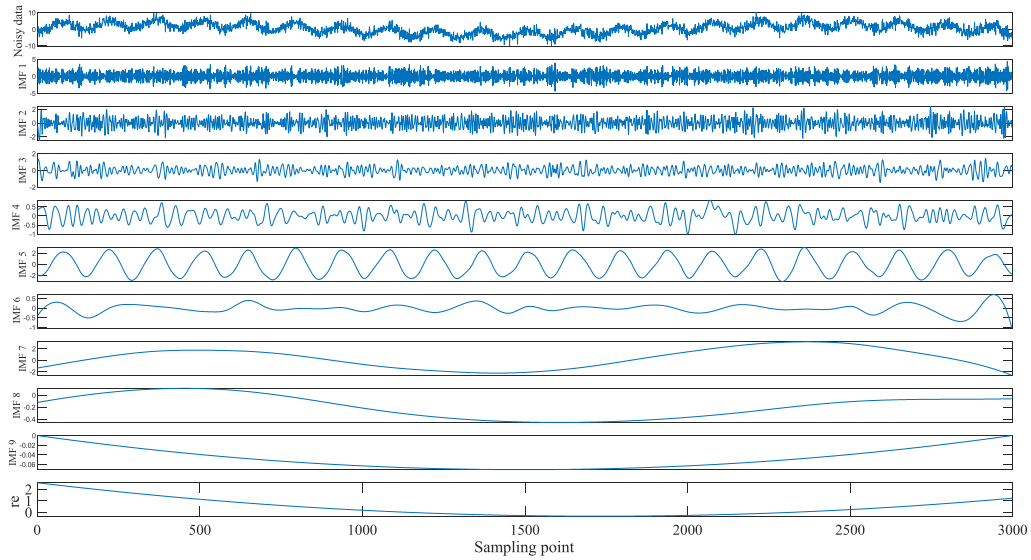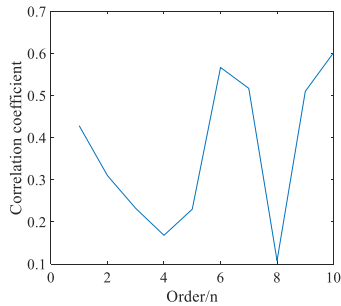
**FIGURE 6.** ICEEMDAN exploded view.



**FIGURE 7.** Changes in IMF correlation coefficients.

$$RMSE = \sqrt{\frac{\sum_{i=1}^{n}(y_i - x_i)^2}{n}} \tag{22}$$

where, $y_i$ denotes the noise-containing signal; $x_i$ denotes the signal after denoising; $n$ denotes the number of signal samples; SNR denotes the ratio of the effective part to the noise part of the signal; and RMSE denotes the difference between the signals before and after denoising; In general, the larger the SNR value and the smaller the RMSE value, the better the denoising effect of the algorithm. Table 1 shows the comparison of the six denoising methods. Table 1 shows the comparison table of six denoising methods, from which we can see that the SNR of 16.8064 of the joint denoising algorithm is higher than that of other algorithms, and the value of RMSE is also gradually reduced to 0.2367, which indicates that the denoising performance is better.

## IV. EXPERIMENTAL VERIFICATION
### A. EXPERIMENT AND SIGNAL ACQUISITION METHOD

In order to verify the superiority and practicability of the combined denoising algorithm for charge induction signals in the process of coal rock fracture, uniaxial compression experiments are conducted on coal rock. The test samples are roof sandstone, coal body, and floor sandstone processed in the laboratory. As required by the International Society of Rock Mechanics for experimental purposes, the composite coal-rock sample was bonded in a 1:1 ratio to a cylindrical shape with a diameter of 50 mm and a height of 100 mm, as shown in Fig. 9. The experimental loading system is composed of SANS universal test press (maximum load is 300 KN), dynamic signal acquisition system, computer, control cabinet, and data acquisition system. A self-developed charge meter was used for charge acquisition, and its charge-voltage conversion ratio was 80~100mV/pC. The experiment was conducted in a self-made electromagnetic shielding chamber, and the experimental system is shown in Fig. 10.

The charge induction signals were collected and analyzed through uniaxial loading experiments on composite coal rock specimens. In order to ensure the universality and accuracy of the experimental results, a total of 21 specimens were made in this study, which were noted as f1-f21, and equally divided into 3 groups, and the experiments were carried out using 3 different loading rates. The loading rates and the corresponding specimen groupings are: 0.1 mm/min (f1-f7), 0.3 mm/min (f8-f14), and 1.0 mm/min (f15-f21).

(1) The composite coal rock sample is fixed between layers; the sample is placed in the shield; the shield is placed on the press test bench; and the charge meter probe is placed in the shield, in the middle of the coal body part, 5 mm away from the sample surface.

(2) Before starting the experiment, power off electrical equipment unrelated to the experiment and other equipment requiring power, and close the laboratory doors and windows to avoid unnecessary movement of personnel so as not to affect the data results.

(3) Turn on the power supply, set the loading rate to 0.1 mm/min, 0.3 mm/min, and 1.0 mm/min, respectively, start the load, charge induction acquisition system, and
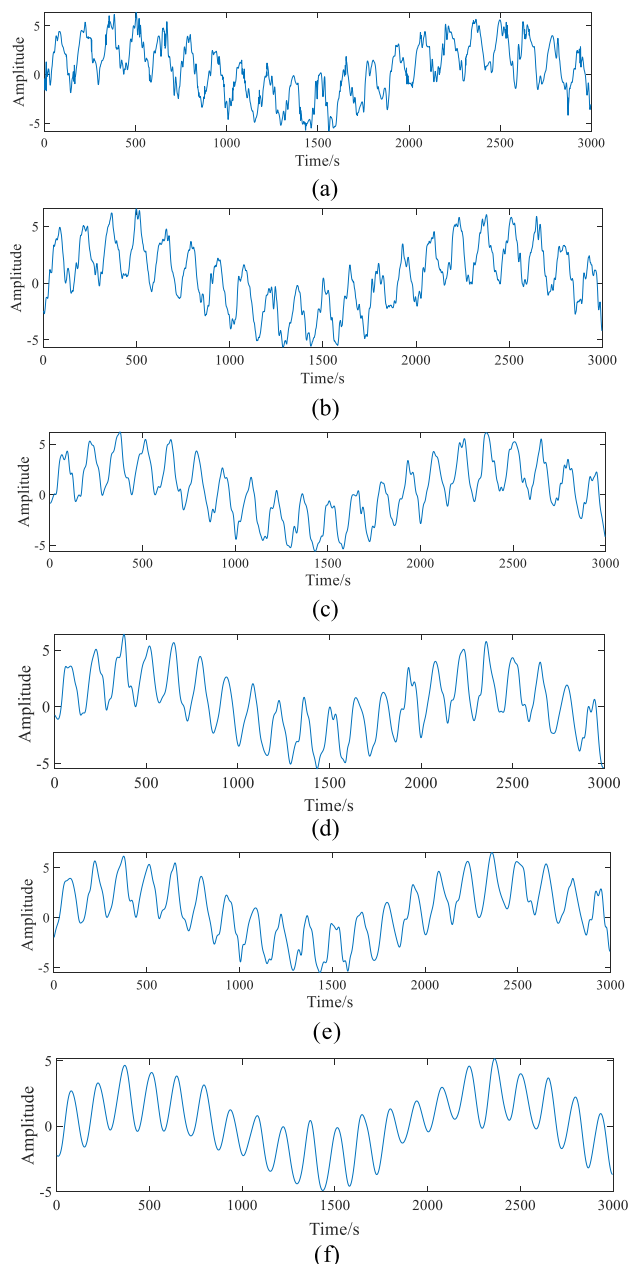
FIGURE 8. Comparison of six denoising algorithms. (a) IWT function denoising. (b) VMD denoising. (c) Joint denoising of IWT and EMD. (d) IEEMDAN denoising. (e) Joint denoising by IWT and EEMD. (f) Joint denoising by IWT function and ICEEMDAN.

electromagnetic radiation acquisition system first, then start the press, start the loading, and record the stress, strain, and charge data.

(4) Observe the loading of coal and rock samples, shut down the experimental system, and save the data after the coal and rock are broken.

## B. ANALYSIS OF EXPERIMENTAL RESULTS

In the experiments, multiple sets of specimens were used for uniaxial loading experiments, and the stress curves of specimens f1, f8 and f15 were selected at uniaxial loading rates of 0.1 mm/min, 0.3 mm/min and 1.0 mm/min. From

TABLE 1. Comparison table of six denoising methods.

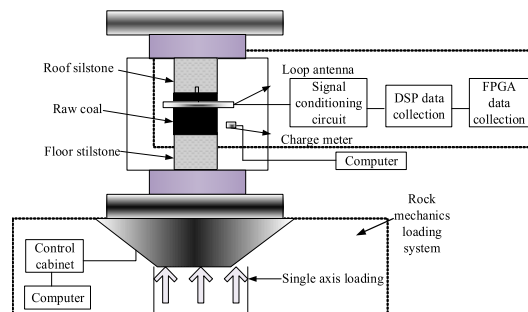| Denoising method | Signal-to-noise ratio（SNR） | Root mean square error（RMSE） |
|---|---|---|
| IWT Function | 14.4582 | 0.3257 |
| IWT functions in conjunction with EMD | 15.8516 | 0.2635 |
| VMD | 16.6385 | 0.2593 |
| ICEEMDAN | 16.6984 | 0.2467 |
| IWT function in conjunction with EEMD | 16.7256 | 0.2416 |
| Joint algorithm of IWT function and ICEEMDAN | 16.8064 | 0.2307 |



FIGURE 9. Composite coal and rock sample.



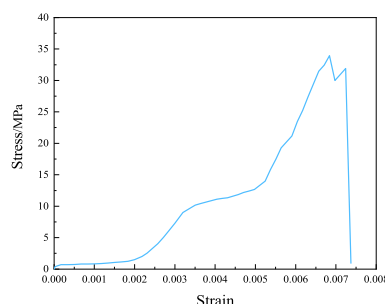FIGURE 10. Experimental system.



FIGURE 11. Coal rock force diagram at loading rate of 1.0mm/min.

Fig. 11, it can be seen that the fracture trends are similar for each coal sample, so only the charge induction signal collected at a loading rate of 0.3 mm/min is shown. As shown in Fig. 14.

As can be seen in Fig. 14, there are more burrs in the original charge-induced signal, which contains serious interference and makes the signal features less pronounced. By combining the signal with the stress data, the variation
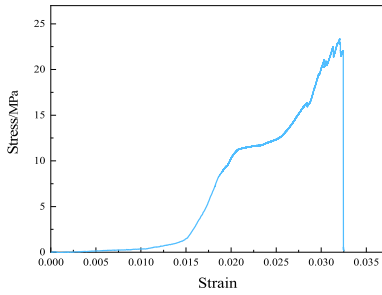
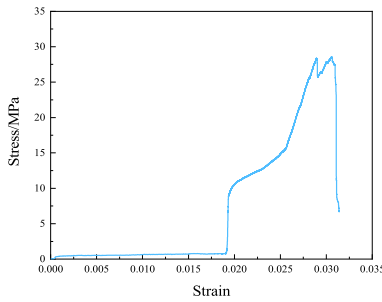**FIGURE 12.** Coal rock force diagram at loading rate of 0.1mm/min.



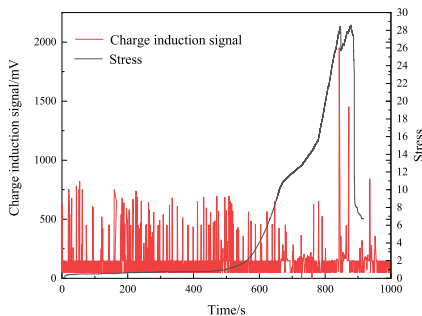**FIGURE 13.** Coal rock force diagram at loading rate of 0.3mm/min.



**FIGURE 14.** Charge induction signal curve.



**FIGURE 15.** Denoising result of charge induced signal. (a) IWT algorithm. (b) IWT function combined with EEMD for denoising. (c) AEEMD-IWT denoising. (d) Joint algorithm of IWT function and ICEEMDAN.

law of the charge signal generated in the process of coal rock fracture cannot be obtained. This is not conducive to the prediction of dynamical disasters in coal and rocks. In order to remove the noise from the signal and to validate the algorithm, improved thresholding algorithm, improved thresholding function and EEMD combined algorithm are used, AEEMD-IWT denoising algorithm, improved threshold function and ICEEMDAN joint algorithm are used to process the charge induction signals, and the results are shown in Fig. 15:

Compared with Fig. 15, it can be seen that the burrs of the charge-induced signal are gradually reduced after denoising, and the overall picture is smoother. The improved threshold function shown in Fig. 15 (a) still contains a lot of noise after de-noising, which cannot accurately reflect the variation trend of signal with loading stress. It can be seen from Fig. 15 (b) - (c) that the denoising effect of the improved threshold function combined with the EEMD algorithm and the AEEMD-IWT denoising algorithm is improved. However, they have the disadvantage that the effective signal is lost and the obtained signal is incomplete. This has a significant impact on analyzing the characteristics of charge
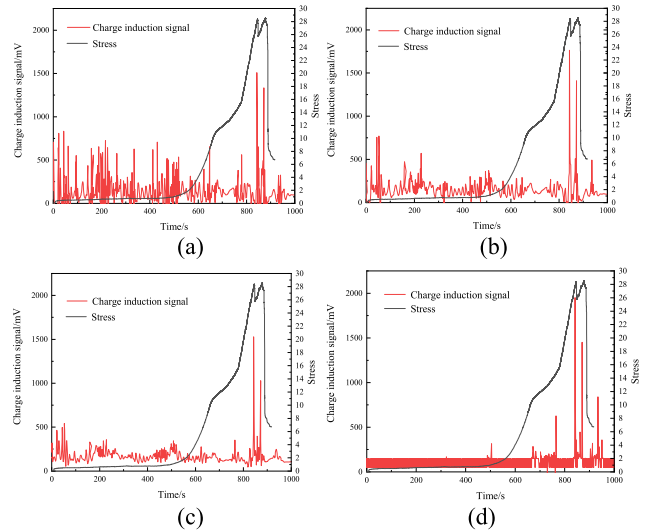
induction signals during the process of coal rock fracture under load. As shown in Fig. 15 (d), the signal denoised by the improved threshold function combined with ICEEM-DAN is clear and complete, and the prediction characteristics of charge signal are obvious. The sudden increase of the charge-induced signal just a few seconds before the peak loading stress of the coal rock can be taken as an omen of the coal rock breaking. Therefore, this algorithm has the best denoising effect and is able to recover the charge-induced signal more accurately.

In order to more intuitively show the superiority of the joint algorithm highlighted in this paper, the noise-to-noise ratio (Rnn) is calculated on the signal [42], and the results are shown in Table 2. The noise-to-noise ratio is the relationship between the removed noise and the original noise. When the noise-to-noise ratio is greater than 0, it indicates that the noise in the signal is not cleanly removed; when the noise-to-noise ratio is less than 0, it indicates that the signal is in a distorted state. Only when the noise-to-noise ratio is close to 0, it indicates that the noise in the signal is removed cleanly and the denoising effect is better.

By comparison, it can be seen that all the above four methods have a denoising effect on the charge induc-tion signals, and their denoising ability is from small to large, as in Improved Threshold Function Denoising, Improved Threshold Function and EEMD Combined Denois-ing, AEEMD-IWT Denoising Algorithm, and IWT Function and Combined Denoising in the order of smallest to largest. There are more burrs in the original charge induction signal, and after a single improved threshold and improved threshold function combined denoising process with EEMD, the signal interference is significantly reduced, but it does not meet the expectations. The charge induction signal is filtered out of most of the burrs in the signal by the AEEMD-IWT joint denoising, and at this time, the noise-to-noise ratio of the

**TABLE 2.** Comparison table of four denoising methods.

| Denoising algorithm | Rnn |
|---|---|
| IWT algorithm | 3.241 |
| IWT function combined with EEMD for denoising | 2.752 |
| AEEMD-IWT denoising | 0.254 |
| Joint algorithm of IWT function and ICEEMDAN | 0.129 |



**FIGURE 16.** On-site signal.



**FIGURE 17.** On-site charge induction signal denoising result diagram. (a) IWT algorithm. (b) IWT function combined with EEMD for denoising. (c) AEEMD-IWT denoising. (d) Joint algorithm of IWT function and ICEEMDAN.

**TABLE 3.** Comparison of standard deviations of four denoising algorithms.

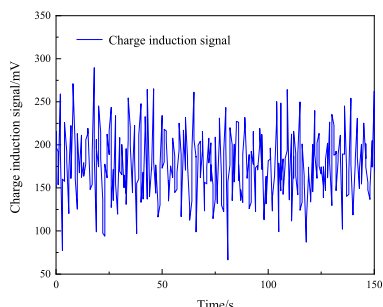| Denoising algorithm | Standard deviation |
|---|---|
| IWT algorithm | 24.3852 |
| IWT function combined with EEMD for denoising | 18.1260 |
| AEEMD-IWT denoising | 15.1506 |
| Joint algorithm of IWT function and ICEEMDAN | 11.0243 |

algorithm is 0.254, whereas after the improved threshold function and the ICEEMDAN joint denoising algorithm, the burrs in the signal are greatly reduced, and the noise-to-noise ratio is only 0.129, which is smaller than the other three denoising algorithms and close to 0. It can be seen that the joint denoising algorithm proposed in this paper has a very good noise reduction effect.

As shown in Fig. 15(d), the improved algorithm significantly reduces the noise content in the signal after denoising, and the charge induction signal is relatively stable during the early stages of coal-rock loading until a significant increase occurs just before coal-rock fracture. Based on the stress curve, it can be seen that the stress peaks at 836s and the coal-rock sample cracks. The charge induction signal is significantly increased in the seconds before the fracture, which can serve as a precursor to the fracture.

By comparison, it can be seen that the proposed algorithm achieves excellent denoising performance on the noisy signals measured in the experiment. Due to the fact that the interference of the signals collected in the compound coal-rock loading experiment mainly comes from the experimental environment, the sources of interference are limited compared to the coal mine site and the signal is less affected. The signals obtained from on-site monitoring in coal mines are affected by multiple factors such as dust, vibrations and electromagnetic interference, resulting in a high noise content in the signals. To verify the reliability and stability of the modified algorithm, the field signal of a section of coal rock before fracture was selected for de-noising verification, as shown in Fig. 16. The denoising results are shown in Fig. 17. The effectiveness of the modified threshold function and the joint ICEEMDAN algorithm is again verified by comparison.

Four denoising algorithms are used to denoise the on-site signal. It can be seen from Fig. 17(a)-(d) that the amplitude change of the charge-induced signal of the four algorithms
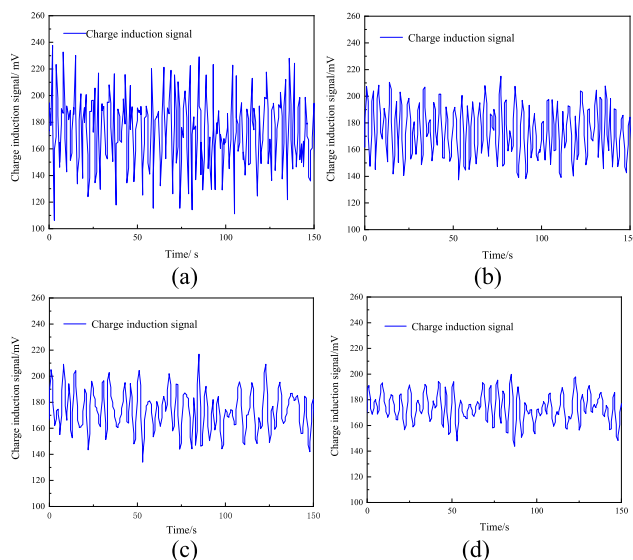
gradually decreases. In order to more clearly compare the denoising results of the on-site signals, their standard deviations are calculated as shown in Table 3. After combining the modified threshold function with ICEEMDAN, the signal standard deviation is minimized, the signal is clearer and smoother, and the denoising is better. The charge-induced signal is less affected during the stress in the coal rock, which is in a normal state with no fracture features. The denoising results of the on-site signals are in good agreement with those collected in the coal and rock loading experiments, which can further verify the effectiveness and accuracy of the combined algorithm.

## V. CONCLUSION

(1) A combined denoising algorithm based on the improved threshold function and ICEEMDAN is proposed, which solves the mode aliasing phenomenon of the EMD algorithm and is adaptive to the signal. At the same time, the computation amount and signal smoothness of the hard threshold are optimized, and the signal distortion of the soft threshold function is solved.

(2) The improved threshold function and ICEEMDAN joint denoising algorithm have good noise reduction

performance for simulation signals. By using six methods such as the IWT function, CEEMD, IWT, and EMD joint denoising algorithms for denoising comparison verification, The results show that the SNR of the combined algorithm is 16.8064. Compared with other algorithms, the SNR has the maximum increase of 16.2%, the RMSE of 0.2307, and the RMSE of other algorithms has the maximum decrease of 29.2%, and the denoising effect is the best among the comparison algorithms.

(3) By conducting uniaxial compression experiments on coal rock samples and comparing the denoising effects of various algorithms on electromagnetic radiation signals generated during the coal rock fracture process. It is found that the noise ratio of the improved threshold function and ICEEMDAN combined algorithm is the smallest, close to 0, and has an obvious denoising effect on simulation signals, which validates the feasibility of this algorithm.

## REFERENCES

[1] Z. Q. Liao, D. C. Chen, and S. W. Liu, "Research of underground electromagnetic interference sources and anti-interference technology," *Ind. Mine Autom.*, vol. 7, no. 7, pp. 25–28, Jul. 2012.

[2] J. H. Chen, W. G. Chou, X. W. Zhao, and H. L. Wang, "Vibration characteristics analysis of the metro tunnel subarea blasting based on wavelet packet technique," *J. Vib. Shock*, vol. 41, no. 6, pp. 222–228, 2022.

[3] W. H. Yi, L. S. Liu, L. Yan, and B. B. Dong, "Vibration signal de-noising based on improved EMD algorithm," *Explos. Shock Waves*, vol. 40, no. 9, pp. 77–87, 2020.

[4] L. Li, J. P. Liu, and W. Wei, "Signal processing method on ultrasonic echo from coal-rock interface based on EWT," *J. China Coal Soc.*, vol. 44, pp. 370–377, Aug. 2019.

[5] S. Y. He, G. Y. Li, H. J. Liu, and L. J. Dong, "Application and research of optimal wavelet base selection method in seismic data processing," *South China J. Seismol.*, vol. 39, no. 3, pp. 49–56, Sep. 2019.

[6] S. Xue, J. Tan, L. Shi, and J. Deng, "Rope tension fault diagnosis in hoisting systems based on vibration signals using EEMD, improved permutation entropy, and PSO-SVM," *Entropy*, vol. 22, p. 209, Feb. 2020.

[7] J. Hou, Y. Wu, H. Gong, A. S. Ahmad, and L. Liu, "A novel intelligent method for bearing fault diagnosis based on EEMD permutation entropy and GG clustering," *Appl. Sci.*, vol. 10, no. 1, p. 386, Jan. 2020.

[8] F. Liu, J. Gao, and H. Liu, "The feature extraction and diagnosis of rolling bearing based on CEEMD and LDWPSO-PNN," *IEEE Access*, vol. 8, pp. 19810–19819, 2020.

[9] D. Yang, Y. Sun, and K. Wu, "Research on CEEMD-AGA denoising method and its application in feed mixer," *Math. Problems Eng.*, vol. 2020, pp. 1–9, Jan. 2020.

[10] B. Xie, Z. Xiong, Z. Wang, L. Zhang, D. Zhang, and F. Li, "Gamma spectrum denoising method based on improved wavelet threshold," *Nucl. Eng. Technol.*, vol. 52, no. 8, pp. 1771–1776, Aug. 2020.

[11] G. Y. Li, S. Y. Yan, X. Y. Wang, J. Y. Lv, S. Z. Liu, and H. L. Wang, "Research on wavelet packet denoising technology for transformer partial discharge," *Heilongjiang Electr. Power*, vol. 45, no. 1, pp. 74–77, Feb. 2023.

[12] Y. Gu, H. J. Xie, L. Li, and G. Li, "Denoising of transient electromagnetic data based on wavelet packet-neural network algorithm," *Coal Eng.*, vol. 55, no. 5, pp. 147–152, 2023.

[13] F. M. Bayer, A. J. Kozakevicius, and R. J. Cintra, "An iterative wavelet threshold for signal denoising," *Signal Process.*, vol. 162, pp. 10–20, Sep. 2019.

[14] T. P. Deng and G. C. Zhang, "Research and application of the new function of wavelet threshold in image denoising," *Modern Electron. Tech.*, vol. 46, pp. 55–60, May 2023.

[15] Y. Zhang, W. Ding, Z. Pan, and J. Qin, "Improved wavelet threshold for image de-noising," *Frontiers Neurosci.*, vol. 13, p. 39, Feb. 2019.

[16] A. Kumar, H. Tomar, V. K. Mehla, R. Komaragiri, and M. Kumar, "Stationary wavelet transform based ECG signal denoising method," *ISA Trans.*, vol. 114, pp. 251–262, Aug. 2021.

[17] J. Zhong, X. Bi, Q. Shu, D. Zhang, and X. Li, "An improved wavelet spectrum segmentation algorithm based on spectral kurtogram for denoising partial discharge signals," *IEEE Trans. Instrum. Meas.*, vol. 70, pp. 1–8, 2021.

[18] S. Hou and W. Guo, "Optimal denoising and feature extraction methods using modified CEEMD combined with duffing system and their applications in fault line selection of non-solid-earthed network," *Symmetry*, vol. 12, no. 4, p. 536, Apr. 2020.

[19] Y. Jia, G. Li, X. Dong, and K. He, "A novel denoising method for vibration signal of hob spindle based on EEMD and grey theory," *Measurement*, vol. 169, Feb. 2021, Art. no. 108490.

[20] T. Jin, Q. Li, and M. A. Mohamed, "A novel adaptive EEMD method for switchgear partial discharge signal denoising," *IEEE Access*, vol. 7, pp. 58139–58147, 2019.

[21] X. Cheng, J. Mao, J. Li, H. Zhao, C. Zhou, X. Gong, and Z. Rao, "An EEMD-SVD-LWT algorithm for denoising a LiDAR signal," *Measurement*, vol. 168, Jan. 2021, Art. no. 108405.

[22] X. Dao, M. Gao, and C. Li, "Adaptive modulation interval filtering algorithm based on empirical mode decomposition," *Measurement*, vol. 141, pp. 277–286, Jul. 2019.

[23] W. Zhang, F. Teng, J. Li, Z. Zhang, L. Niu, D. Zhang, Q. Song, and Z. Zhang, "Denoising method based on CNN-LSTM and CEEMD for LDV signals from accelerometer shock testing," *Measurement*, vol. 216, Jul. 2023, Art. no. 112951.

[24] B. Li, L. Zhang, Q. Zhang, and S. Yang, "An EEMD-based denoising method for seismic signal of high arch dam combining wavelet with singular spectrum analysis," *Shock Vibrat.*, vol. 2019, pp. 1–9, Mar. 2019.

[25] L. Xiong, X. Gong, Y. Liang, and X. Ran, "Research on speech noise reduction based on VDM and wavelet threshold," *Electron. Qual.*, vol. 44, no. 5, pp. 68–72, Mar. 2023.

[26] Z. Sun, X. Xi, C. Yuan, Y. Yang, and X. Hua, "Surface electromyography signal denoising via EEMD and improved wavelet thresholds," *Math. Biosci. Eng.*, vol. 17, no. 6, pp. 6945–6962, 2020.

[27] L. Feng, J. Li, C. Li, and Y. Liu, "A blind source separation method using denoising strategy based on ICEEMDAN and improved wavelet threshold," *Math. Problems Eng.*, vol. 2022, pp. 1–9, Feb. 2022.

[28] L. Yuan, E. Y. Wang, Y. K. Ma, Y. B. Liu, and X. L. Li, "Research progress s of coal and rock dynamic disasters and scientific and technological problems in China," *J. China Coal Soc.*, vol. 48, no. 5, pp. 1825–1845, 2023.

[29] H. L. Huang, Q. F. Li, B. Y. Li, H. Wu, and P. Tang, "Dynamic rupture of rocks and analysis of their electromagnetic radiation signal characteristics," *Miner. Eng. Res.*, vol. 38, no. 4, pp. 51–59, Dec. 2023.

[30] Z. Yang, Q. J. Qi, and X. Li, "New signal denoising algorithm of loading coal-rock electromagnetic emission," *Transducer Microsyst. Technol.*, vol. 36, no. 3, pp. 132–135, Mar. 2017.

[31] M. Safta, P. Svasta, and M.-O. Dima, "Wavelet signal denoising applied on electromagnetic traces," in *Proc. IEEE 23rd Int. Symp. Design Technol. Electron. Packag. (SIITME)*, Oct. 2017, pp. 399–402.

[32] Q. Wu, Y. Ma, D. Li, Y. Wang, and Y. Ji, "Denoising algorithm of ground-airborne time-domain electromagnetic method based on variational Bayesian-based adaptive Kalman filter (VBAKF)," *J. Appl. Geophys.*, vol. 202, Jul. 2022, Art. no. 104674.

[33] S.-H. Chen and E.-Y. Wang, "Removal of noises from electromagnetic radiation of coal or rock with EEMD-adaptive morphological filter," *J. Coal Sci. Eng.*, vol. 18, no. 3, pp. 330–336, Aug. 2012.

[34] S.-Y. Liu, Z.-L. Ouyang, G. Chen, X. Zhou, and Z.-J. Zou, "Black-box modeling of ship maneuvering motion based on Gaussian process regression with wavelet threshold denoising," *Ocean Eng.*, vol. 271, Mar. 2023, Art. no. 113765.

[35] S. Wang, D. Meng, and K. Zhang, "Study on the application of wavelet threshold denoising in the detection of coal spectra by LIBS," *J. Phys., Conf.*, vol. 2396, no. 1, Dec. 2022, Art. no. 012024.

[36] H. Ma, Y. Cheng, F. Cai, L. Zhang, and Z. Shen, "Application of improved wavelet threshold denoising method in motor current signal processing," *Mech. Electr. Eng. Technol.*, vol. 51, no. 11, pp. 55–57, 2022.

[37] Y. Hou, S. Li, H. Ma, S. Gong, and T. Yu, "Weak signal detection based on lifting wavelet threshold denoising and multi-layer autocorrelation method," *J. Commun.*, vol. 17, no. 11, pp. 890–899, Nov. 2022.

[38] F. Wang, J. Cen, Z. Yu, S. Deng, and G. Zhang, "Research on a hybrid model for cooling load prediction based on wavelet threshold denoising and deep learning: A study in China," *Energy Rep.*, vol. 8, pp. 10950–10962, Nov. 2022.

[39] R. Shi, "Analysis of image denoising algorithm based on new wavelet threshold function," *Electron. Technol.*, vol. 51, no. 9, pp. 46–48, Sep. 2022.

[40] M. A. Colominas, G. Schlotthauer, and M. E. Torres, "Improved complete ensemble EMD: A suitable tool for biomedical signal processing," *Biomed. Signal Process. Control*, vol. 14, pp. 19–29, Nov. 2014.

[41] X. Li, H. Li, Z. Yang, J. Zhou, H. Li, and J. Bu, "Radiation signal denoising method of loaded coal-rock based on ICEEMDAN-PCK-means-IP," *IEEE Sensors J.*, vol. 23, no. 19, pp. 23103–23118, Oct. 2023.

[42] C. Li, L. Dong, Q. Wang, F. Wang, P. Hu, and X. Xu, "Noise auto identification and de-noising method of coal-rock weak electromagnetic signals," *J. China Coal Soc.*, vol. 41, no. 8, pp. 1933–1940, Aug. 2016.

**HAO LI** was born in Dandong, Liaoning, China, in 1997. He received the B.S. degree in electrical engineering and automation and the M.S. degree in electrical engineering from Liaoning Technical University, Huludao, China, in 2019 and 2021, respectively, where he is currently pursuing the Ph.D. degree. His main research interests include the study of the electromagnetic theory of mines, the dynamic disaster of coal and rock prevention, and engineering electromagnetic field theory. His awards and honors include the National Scholarship for Postgraduate Students (Ministry of Education of China) and the Science and Technology Second Prize (China Federation of Commerce).
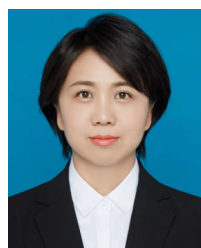
**XIN LI** was born in Fuxin, Liaoning, China, in 1981. She received the B.S. degree in automation, the M.S. degree in control theory and control engineering, and the Ph.D. degree in management science and engineering from Liaoning Technical University, Huludao, China, in 2003, 2006, and 2016, respectively. Currently, she is a Professor with Liaoning Technical University. Her main research interests include the study of the electromagnetic theory of mines, the dynamic disaster of coal and rock prevention, and ultra-wideband radar detection technology. She is a member of the 3rd China Mechanical Industry Education Association (CMIE) Electrical Engineering and Automation Sub-Committee.
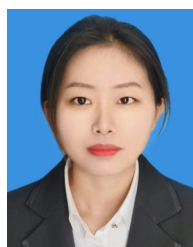
**HUI ZUO** received the master's degree from Liaoning Technical University, Huludao, China, in 2023. Her main research interests include mine electrical theory and new technology.
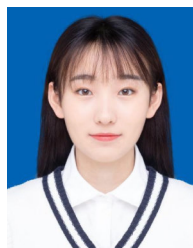
**JINGRAN BU** received the B.S. degree in electrical engineering and automation from Bohai University, Jinzhou, China, in 2022. She is currently a Graduate Student with Liaoning Technical University, Huludao, China. Her main research interests include the study of the electromagnetic theory of mines, electromagnetic signal detection technique, and mine physical network technology.
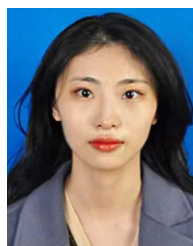
**YUNING WANG** received the master's degree from Liaoning Technical University, Huludao, China, in 2023. Her main research interests include mine electrical theory and new technology.

**ZHEN YANG** received the B.S. degree in automation, the M.S. degree in power electronics and transmission, and the Ph.D. degree in safety technology and engineering from Liaoning Technical University, Huludao, China, in 2002, 2006, and 2016, respectively. He is currently a Professor, a Candidate of the "Thousand" Level of Liaoning BaiQianWang Talents Project, and the Vice President of the College of Electrical and Engineering Control, Liaoning Technical University. His main research interests include the study of the electromagnetic theory of mines, the dynamic disaster of coal and rock prevention, and ultra-wideband radar detection technology. His awards and honors include the second and third prizes of the Science and Technology Award (China Federation of Industry and Commerce) and the first Youth May 4th Medal (Liaoning Technical University).

**JING ZHOU** received the B.S. degree in electrical engineering and its intelligent control from Liaoning Technical University, Huludao, China, in 2022, where she is currently pursuing the degree. Her main research interests include the study of the electromagnetic theory of mines and ultra-wideband radar detection technology. Her awards and honors include the Outstanding Graduate (Education Department of Liaoning Province) and the First Class Scholarship for Postgraduate Admission (Liaoning Technical University).

● ● ●